Statistics and characteristics of xuv transition arrays from laser-produced plasmas of the elements tin through iodine

Winnie Svendsen* and Gerard O'Sullivan

Physics Department, University College Dublin, Belfield, Dublin 4, Ireland

(Received 7 February 1994; revised manuscript received 13 June 1994)

Spectra of laser-produced plasmas of the elements from tin to iodine contain weak bands of quasicontinuum overlaid by weak emission lines in the 70–120-Å region. Multiconfiguration-Dirac-Fock calculations show that these features are consistent with theoretical spectra for $4d^N$-$4d^{N-1}(5f+6p)$ transitions in a number of adjacent ion stages which are predicted to produce unresolved transition arrays (UTA) in this spectral region. Moreover, the calculations predict a gradual decrease of $4d$-$5f$ oscillator strength with increasing ionization up to the eleventh spectrum where $\sum gf(4d$-$5f) \approx 0$. However, inclusion of configuration interaction effects between the $4d^9nf$ levels showed that $4d^94f$ and $4d^95f$ mixing shifts this minimum to the thirteenth spectrum. The theoretical data were then parametrized within the UTA formalism and the different order moments corresponding to weighted mean energy, variance, and skewness coefficient evaluated.

INTRODUCTION

Spectra recorded when a Q-switched solid-state laser pulse is focused onto targets of tin, antimony, or tellurium at power densities in the 10^{15}–10^{16} Wm^{-2} range consistently contain weak bands of emission in the 60–100-Å region superimposed on the recombination background. Comparison with well-documented spectra obtained under identical conditions and calculations performed within the collisional radiative plasma model both indicate that ion stages up to the fifteenth or higher are present in the emitting plasma [1,2]. The ground configurations of these ions typically contain open $5p$, $5s$, and $4d$ subshells. Level energies of these ions up to the third spectrum have been tabulated [3], while some data on the Cd- and In-like ions Te IV and Te V, and I V and I VI have also been reported [4–6]. In the Ag I sequence (ground configuration $4d^{10}5s$) many levels of the type $4d^{10}nl$ have been determined [3,7], while the core excited transitions $4d^{10}5s$-$4d^95s5p$ have also been observed [8,9]. In the Pd I sequence (ground state $4d^{10}$ $^1S_0$), $4d^{10}$-$4d^94f$ and $4d^95p$ transitions have been assigned in Sn V [10,11], Sb VI, Te VII [12], and I VII [13]. In addition, the $4d^96p$ levels of Sb VI and Te VII and $4d^95f$ levels of I VIII were deduced in these studies. Transitions based on open $4d$ subshell configurations have not been extensively studied for this group of elements with the notable exception of the $4d^9$-$4d^85p$ of the Rh I sequence, which has been analyzed for all of the present elements [10–15]. To our knowledge, no detailed classification of transitions of the type $4d^N$-$4d^{N-1}5f$ or $4d^N$-$4d^{N-1}6p$ have been reported for $N < 10$ although work for $N = 9$ is currently in progress [16]. In this work we show that the weak emission bands observed in the vuv at $\lambda < 100$ Å are consistent with unresolved transition arrays of this type.

EXPERIMENT

Two different lasers were used to produce the spectra: a 1.5-J, 20-ns Q-switched ruby oscillator and a 860-mJ, 12-ns Nd:YAG (yttrium aluminum garnet) oscillator-amplifier system. The ruby pulse was focused to a spot size of approximately 200 μm in diameter, while the Nd:YAG, which has a better mode structure and beam profile, could be focused to a spot diameter of 140 μm, so the average power densities ϕ attained were 2.4×10^{15} and 4.6×10^{15} Wm^{-2}. According to the collisional radiative model for incompletely ionized elements of atomic number A, the average electron temperature T_e(eV) and ionization state Z are given empirically by [2]

$$T_e(\text{eV}) = 5.2 \times 10^6 A^{1/5} [\lambda^2 \phi]^{3/5}$$

and

$$Z = \tfrac{2}{3} [AT_e]^{1/2} \, ,$$

which give values of $T_e = 36$ eV and $Z = 12$ for the ruby pulse and $T_e = 89$ eV and $Z = 15$ for the Nd:YAG pulse. For Sn, Sb, and Te pure metal targets were used to produce spectra, while for iodine, crystalline KI was compressed to form a suitable slab target at a pressure of 2×10^7 kg m^{-2}. The spectra were photographed on Kodak SWR plates on a 2-m grazing incidence spectrograph in which the dispersion varies from 0.78 Å mm^{-1} at 80 Å to 1.2 Å mm^{-1} at 150 Å. Typically, 300 laser shots at a slit to target distance of 10 cm and a slit width of 15 μm were needed to achieve adequate plate blackening. Spectra from Al and BeO targets were superimposed to provide reference spectra of ionized aluminium, beryllium, and oxygen [17]. The photographic plates were subse-

*Present address: Risø National Laboratory, Department of Solid State Physics, 4000 Roskilde, Denmark.

quently scanned using a digital microdensitometer to provide calibrated traces of the spectra.

RESULTS

A. Comparison between experimental data and theoretical predictions

Microdensitometer traces of the spectra obtained for tin, antimony, and tellurium are shown in Fig. 1. However, because of the reduced concentration of iodine ions in the plasma produced on the KI target, the overall spectrum was considerably weaker. Accordingly, it was not possible to identify clearly the positions of the short-wavelength unresolved transition arrays (UTA) and the spectrum is not reproduced here. The spectra are dominated in each case by an intense unresolved transition array which is centered near 137 Å in Sn, 126 Å in Sb, 120 Å in Te, and 113 Å in I. This feature has been previously observed for the elements past iodine [1,18] and has been interpreted as originating from

$$4d^{10}5s^m5p^h\text{-}4p^94f5s^m5p^h$$

and

$$4p^64d^N\text{-}4p^64d^{N-1}4f + 4p^54d^{N+1}$$

transitions [19]. Configuration interaction (CI) between the $4p^64d^{N-1}4f$ and $4p^54d^{N-1}$ was found to yield a spectacular narrowing and energy shift for ionized praeseodymium. An earlier calculation [20] within the UTA framework [21–30] had shown that the general profile of the UTA in cesium could be reproduced by consideration of $4d^N\text{-}4d^{N-1}4f$ transitions alone in a restricted number of ion stages. However, the position of the array shifts towards longer wavelength with increasing ionization which would lead to a greater overall width than observed if all possible ion stages with $4d^N$ ground states (Cs X–Cs XX) were to contribute. The experimental spectrum with which comparison was made only contained stages up to Cs XV or Cs XVI. In the present case calculations were performed both for noninteracting $4d^N\text{-}4d^{N-1}4f$ and $4p^64d^N\text{-}4p^54d^{N+1}$ and with allowance for full CI using the multiconfiguration-Dirac-Fock
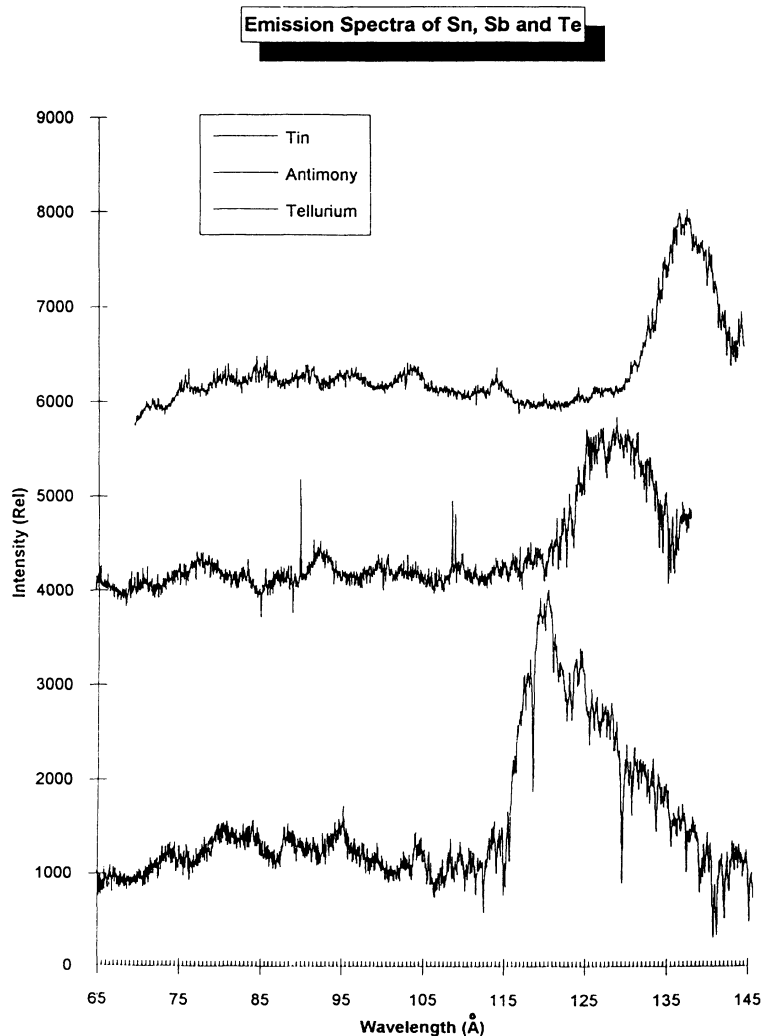
FIG 1. Densitometer traces of the spectra from laser-produced plasmas of tin, antimony, and tellurium. The high-intensity peak arises from $4p^6\text{-}4d^N\text{-}4p^54d^{N+1} + 4p^64d^{N-1}4f$ transitions (see text).

(MCDF) code of Grant *et al.* [31] which showed that CI effects are still important at low Z. A sample of the results of these calculations for Cs is shown in Fig. 2. In obtaining this figure each line was assigned a Gaussian profile with an artificial width of 0.02 Å which is close to the observed spectral linewidth and an intensity proportional to its oscillator strength or gf value (gf denotes the total oscillator strength, i.e., the emission oscillator strength times the statistical weight of the upper state).

Similar line-by-line MCDF calculations were also performed for $4d^N$-$4d^{N-1}5f$ and $6p$ transitions. From these data it was predicted that the intensity of $4d$-$5f$ transitions is almost zero at the XI spectrum in each case due to dipole matrix element cancellation. At precisely the same spectrum, the centers of gravity of the $4d^{N-1}5f$ and $4d^{N-1}6p$ cross, analogous to the behavior observed for the centers of gravity of the $4d^94f$ and $4d^95p$ configurations of the Pd I sequence, which were also observed to cross at Ba XI [32]. At this spectrum there is some evidence of weak configuration mixing, the main effect of which is a redistribution of intensity among the strongest lines of the $4d^N$-$4d^{N-1}6p$ array, while the overall profile and position remain essentially unchanged.

To test the accuracy of the calculations and intensity predictions, comparison was made between the calculated and observed energies for the $4d^{10}$-$4d^95f$ and $4d^96p$ lines of the Pd I sequence. It was found that the accuracy of the $4d$-$6p$ energy prediction improves with increasing ionization and is generally close to 1 eV, while for the $4d$-$5f$ case, the anticipated accuracy is of the order of 2

Wavelength (Å)

Wavelength (Å)
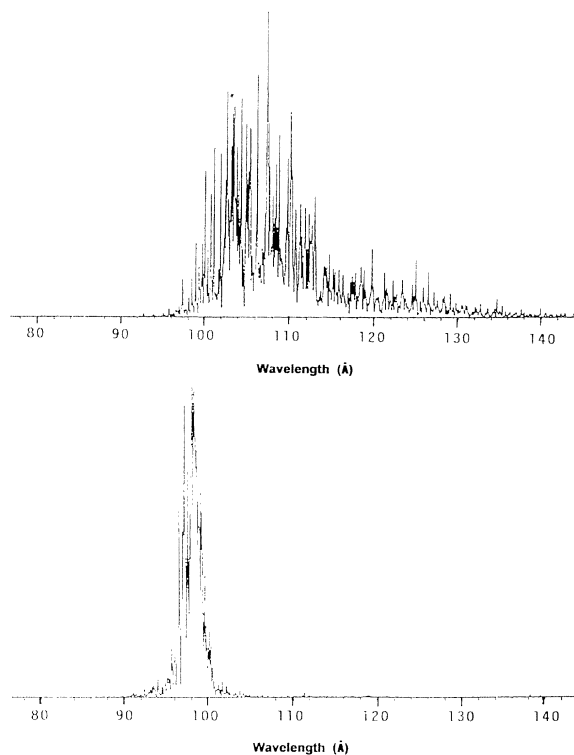
FIG. 2. Configuration interaction effects in Cs XVI: Top, summed spectra of $4p^64d^4$-$4p^54d^5$ and $4p^64d^34f$ without CI, and bottom, spectrum of $4p^64d^4$-$4p^54d^5$+$4p^64d^34f$ with CI included.

eV. Thus it is reasonable to assume that in the general $4d^N$-$4d^{N-1}5f$ case, the accuracy is ±2.0 eV, while for $4d^N$-$4d^{N-1}6p$, it is closer to ±1.0 eV. However, as regards intensities, insufficient experimental data exist to made a meaningful comparison for the $4d$-$6p$ transitions but the gf values for the $4d^{10}$-$4d^95f$ give a good estimate of the observed intensity, so it is reasonable to assume the same is true in the $4d$-$6p$ case.

Moreover, in line with the trend already alluded to, the intensity of the $4d^{10}$-$4d^95f$ lines is predicted to decrease rapidly in proceeding up the sequence and to effectively vanish at Ba XI, where the $5f$ contracts to overlap the $4d$ orbital completely out of phase. It should be noted, however, that in a recent study of $5d^{10}6s \rightarrow 5d^96snf$ and $5d^96snp$ transitions in Pb IV, it was found that the accuracy of the prediction for level lifetimes and transition probabilities for the low-n states improved as an increasing number of high-n states were included explicitly in the calculation [33]. From earlier analysis of $4d^{10}$-$4d^9nf$ transitions along the Xe I isoelectric sequence, it is known that intrachannel mixing among the $4d^9nf$ terms must be included to explain the spectra of Ba III and La IV [34–36]. In the present case addition of the $4d^94f$ configuration to the $4d^9(5f+6p)$ caused the MCDF routine to experience convergence problems. As a result, further calculations were undertaken with the HXR code of Cowan [37]. Three sets of calculations were performed. First, the $4d^{10}$-$4d^9(5f+6p)$ was recalculated for comparison with MCDF results. Apart from a small difference in energies and a summed oscillator strength for $4d$-$5f$ transitions approximately 20% larger, the overall gf-value trend was identical i.e., a sharp minimum at Ba XI and a gradual increase thereafter. Next, the excited-state basis was extended to include all $4d^9np$ levels for $5 \leq n \leq 8$ and all $4d^9nf$ levels for $4 \leq n \leq 10$. This calculation predicted that the $4d$-$5f$ gf-value minimum should be shifted to Pr XIII and be even more pronounced. It also yielded a larger gf value for $4d$-$5f$ transitions earlier in the sequence. These results are presented in Fig. 3 where $4d$-$4f$ oscillator strengths are included for comparison. Also included in this figure are $4d$-$6p$ oscillator strengths which are seen to remain approximately constant along the sequence. It should be noted that the distribution among the individual $4d^{10}$-$4d^96p$ lines was in excellent agreement with the earlier MCDF results. The increase in oscillator strength for $4d$-$5f$ transitions is essentially due to $4d^94f$ and $4d^95f$ mixing. The $4d^94f\,^1P_1$ component of the $4d^95f\,^1P_1$ level decreases from 12% in Sb VII to 4% in Ba XI and is further reduced as one proceeds along the sequence. Since the $4f$ wave function derived in these calculations is effectively a $4f_{av}$ function, i.e., associated with the configuration average rather than the $^1P_1$ term, and since the wave function for the latter is known to have a greater radial extent below the eleventh ion stage, the $4d^{10}$-$4d^94f\,^1P_1$ matrix element and consequently the summed gf $(4d$-$4f)$ value is overestimated here [38–40]. Consequently, $\sum gf(4d$-$5f)$ is also an overestimate and the true value is probably closer to the non-CI one. However, the shift of the minimum position from the eleventh to the thirteenth stage is a genuine effect and the calcula-
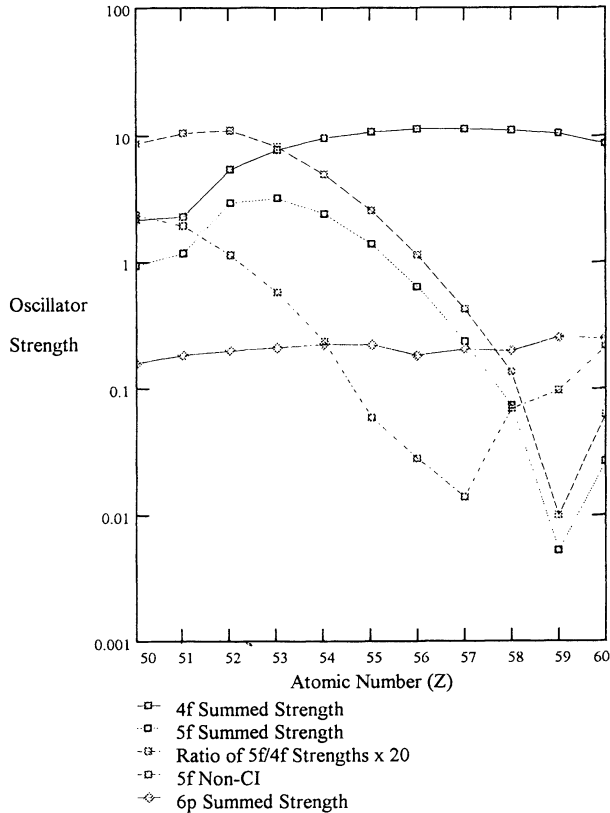
FIG. 3. Summed oscillator strengths for $4d^{10}$-$4d^9nl$ transitions showing the effect of $4d^9(4f+5f)$ interaction on $4d^{10}$-$4d^95f$ oscillator strength.

tions in general imply that most of the observable detail in the spectra past the ninth ion stage (tenth spectrum) arises from $4d^N$-$4d^{N-1}6p$ transitions; below the ninth stage, the $4d^N$-$4d^{N-1}5f$ transitions should dominate. The final calculation again included the same $4d^9nf$ and $4d^9np$ basis with the $4d^94f$ excluded. As expected, the $4d$-$5f$ summed oscillator strength was close to the value obtained in the first calculation though in each case it was slightly reduced due to a loss of strength from mixing with the higher nf states.

At this point it was decided to investigate these predictions experimentally. In Xe IX a line at 128.76 eV was identified as $4d^{10}$-$4d^95f\ ^1P$ [41], which may be compared with an MCDF prediction of 127.476 eV ($\Delta E = 1.284$ eV); however, the measurement accuracy was ±0.05 eV. We obtained additional spectra of Cs, Ba, and La to follow this transition. In Cs we observed a strong line at 146.00±0.05 eV which may be compared with the MCDF value of 144.677 eV. In Ba XI the MCDF value is 162.613 eV which would indicate the presence of the transition at 163.91±0.10 eV. No strong line appears in our spectra at this energy though a feature at 163.83 eV may be a candidate. However, no $4d^{10}$-$4d^95f\ ^1P_1$ line could be located in the La spectrum which would seem to verify the intensity trend predicted from Fig. 3. Since in our spectra ion stage differentiation is not possible, further studies of these spectra would be of interest to fully explore this effect and document its evolution into the lanthanides.

Having thus established that the energy predictions are sufficiently accurate to allow for a meaningful compar-
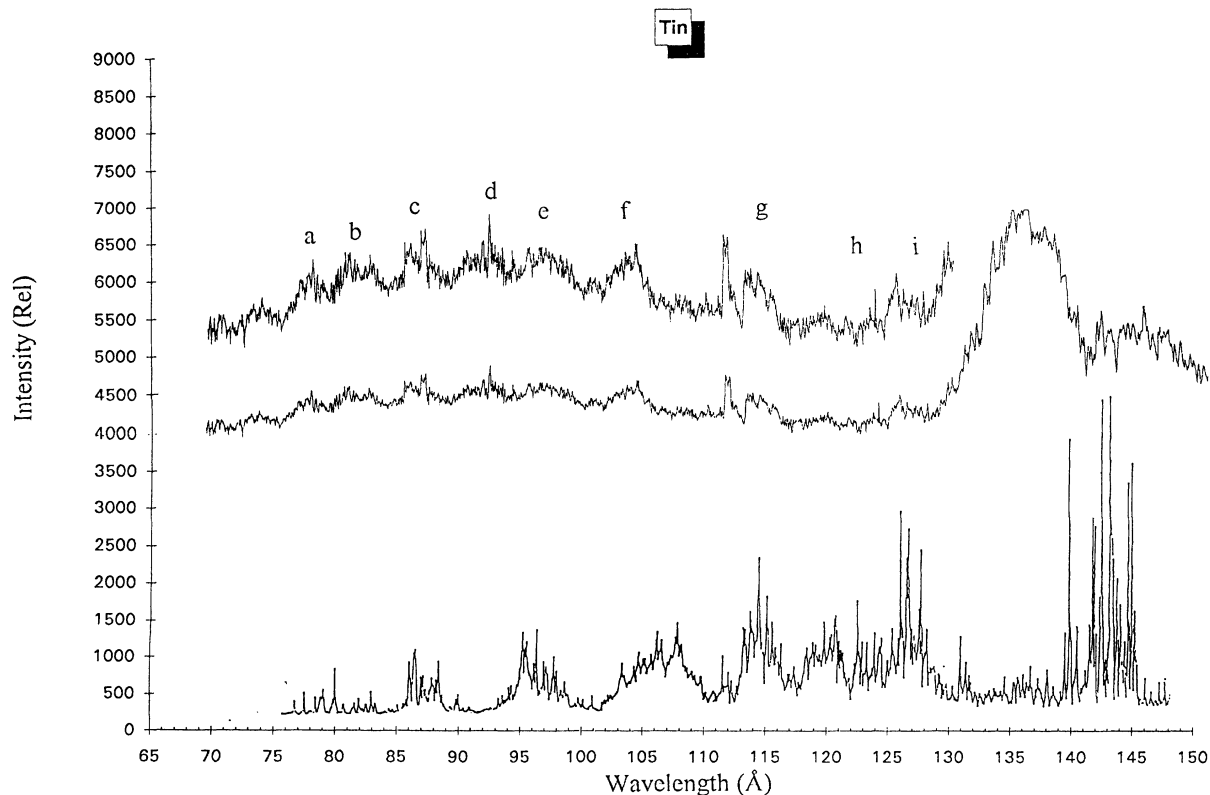
FIG. 4. Comparison between the experimental spectrum of a laser-produced plasma of ionized tin and theoretical $4d^N$-$4d^{N-1}(5f+6p)$ transitions.
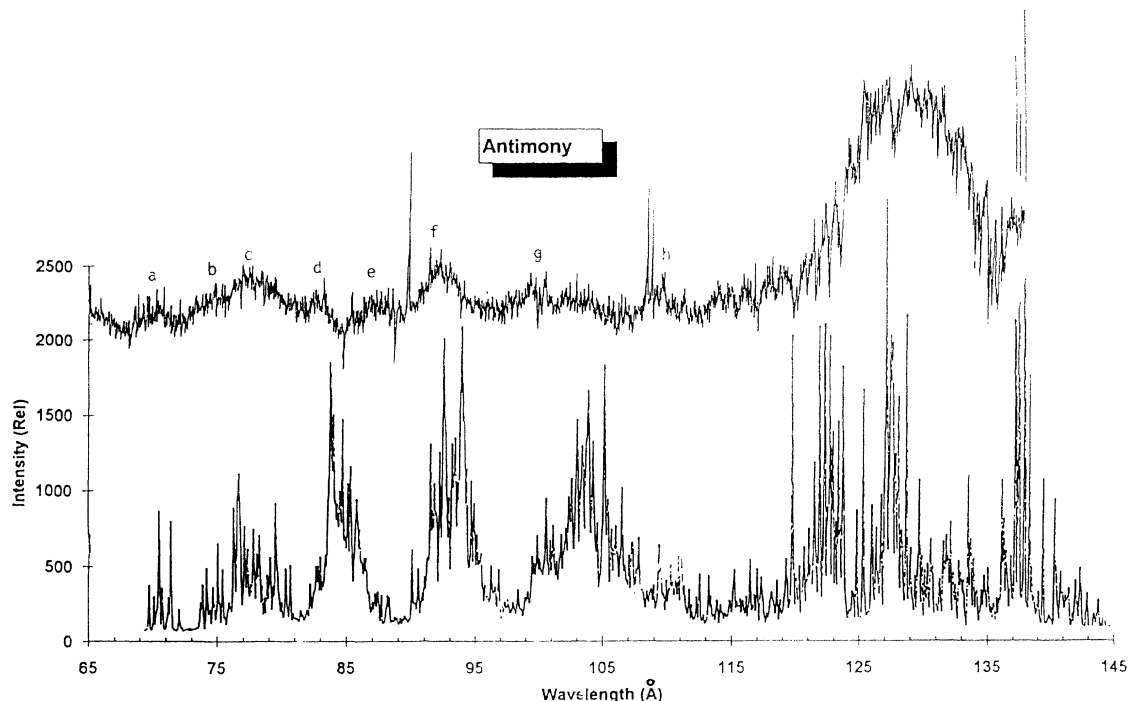
FIG. 5. Comparison between the experimental spectrum of a laser-produced plasma of ionized antimony and theoretical $4d^N$-$4d^{N-1}(5f+6p)$ transitions.

ison, we have attempted to correlate the theoretical and experimental data. Some weak peaks are evident in the spectra of Fig. 1. In Figs. 4–6 these spectra are again presented along with the theoretical $4d^N$-$4d^{N-1}(5f+6p)$ data. No ion stage weighting is incorporated in these theoretical plots. All stages are assumed to be equally populated and the intensities are then taken as being proportional to the gf values. Likewise, plasma opacity effects were not included but these are expected to be rel-

atively unimportant because of the overall weakness of the transitions. A comparison between the observed and theoretical peaks is presented in Table I. The experimental peak centers are quoted to an accuracy of $\sim \pm 1.0$ Å because the exact center point is difficult to locate due to their inherent weakness. It is seen that the overall agreement is excellent, in general to within ± 1 Å, in line with the limits of both the experimental and theoretical accuracy.
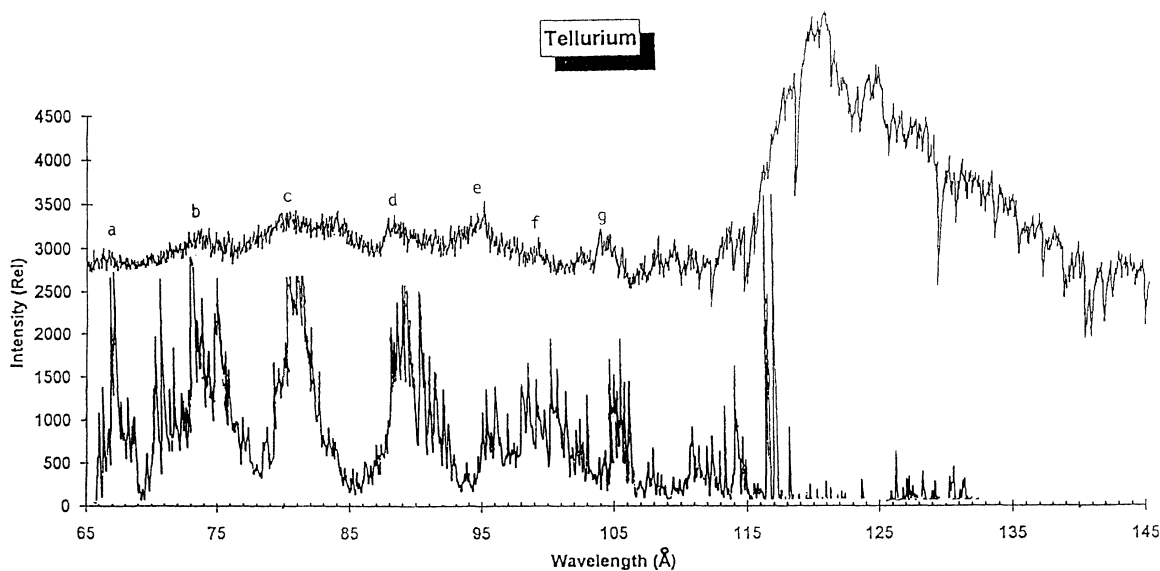
FIG. 6. Comparison between the experimental spectrum of a laser-produced plasma of ionized tellurium and theoretical $4d^N$-$4d^{N-1}(5f+6p)$ transitions.

B. Statistical parametrization of the UTA

Although line-by-line calculations have been performed for all of the transitions $4d^N\text{-}4d^{N-1}(5f+6p)$ for $1 \le N \le 10$, because of the line density and low energy resolution, no attempt was made to identify individual spectra lines. For N values in the range 3–7, such identification is virtually impossible anyway. Consequently, we choose to describe the UTA within the formalism of Bauch-Arnoult et al. [21–27], who showed that various moments of the array could be used to parameterize it. The general nth moment for transitions between configurations a and b is given by

$$\mu_n(a-b) = \frac{\sum_{m,m'} [\langle m'|H|m'\rangle - \langle m|H|m\rangle]^n |\langle m|D|m'\rangle|^2}{\sum_{m,m'} |\langle m|D|m'\rangle|^2},$$

where D is the electric dipole operator and the sum runs over all states m and m' of configurations a and b, respectively.

Since

$$f_{m,m'} \propto [\langle m'|H|m'\rangle - \langle m|H|m\rangle]|\langle m|D|m'\rangle|^2,$$

$$\mu_n(a-b) = \frac{\sum_{m,m'} g_m f_{mm'}[\langle m'|H|m'\rangle - \langle m|H|m\rangle]^{n-1}}{\sum_{m,m'} g_m f_{mm'}[\langle m'|H|m'\rangle - \langle m|H|m\rangle]^{-1}}.$$

The first moment μ_1 gives the average value of the weighted mean energy of the UTA. The variance V is the centered second-order moment μ_2^c and is given by $V = \mu_2 - (\mu_1)^2$ and is related to the width of the array. For a normal distribution the full width at half maximum is $\Delta E = \sqrt{2}\ln 2\sigma$ ($\sigma^2 = V$). The skewness, or asymmetry, of the distribution can be described by the skewness

TABLE I. Observed and calculated wavelengths for $4d^N\text{-}4d^{N-1}(5f+6p)$ arrays of Sn, Sb, and Te.

Element		Observed Array			Calculated weighted mean (Å)	
		Center (Å)	Range (Å)	Transition	of component arrays	Ion
Sn	a	75	(74–76)	$4d$-$6p$	73.20	XIV
	b	80	(78–83)	$4d$-$5f$	77.80	XIV
				$4d^2$-$4d6p$	80.05	XIII
	c	85	(83–87)	$4d^2$-$4d5f$	83.18	XIII
	d	90	(88–92)	$4d^3$-$4d^26p$	87.97	XII
				$4d^3$-$4d^25f$	89.96	XII
	e	96	(93–98)	$4d^4$-$4d^35f$	96.96	XI
				$4d^4$-$4d^36p$	97.25	XI
	f	103	(101–106)	$4d^5$-$4d^45f$	105.65	X
				$4d^5$-$4d^46p$	108.51	X
	g	114	(111–117)	$4d^6$-$4d^55f$	116.14	IX
	h	125	(124–126)	$4d^6$-$4d^56p$	122.35	IX
	i	127	(126–130)	$4d^7$-$4d^65f$	129.17	VII
Sb	a	70	(68–72)	$4d$-$5f$	70.28	XV
				$4d$-$6p$	70.97	XV
	b	74	(72–75)	$4d^2$-$4d5f$	74.75	XIV
	c	78	(76–81)	$4d^2$-$4d6p$	77.41	XIV
				$4d^3$-$4d^25f$	80.01	XIII
	d	83	(82–84)	$4d^3$-$4d^26p$	84.84	XIII
	e	87	(85–89)	$4d^4$-$4d^35f$	86.90	XII
	f	92	(90–94)	$4d^5$-$4d^45f$	92.94	XI
				$4d^4$-$4d^36p$	93.77	XII
	g	103	(97–106)	$4d^6$-$4d^55f$	101.21	X
				$4d^5$-$4d^46p$	104.37	XI
	h	109	(107–112)	$4d^7$-$4d^65f$	110.71	IX
Te	a	66	(65–68)	$4d^2$-$4d5f$	67.63	XV
				$4d^3$-$4d^26p$	68.74	XIV
	b	74	(71–76)	$4d^3$-$4d^25f$	72.02	XIV
				$4d^4$-$4d^36p$	74.80	XIII
	c	82	(77–87)	$4d^4$-$4d^35f$	76.95	XIII
				$4d^5$-$4d^45f$	81.91	XII
				$4d^5$-$4d^46p$	82.12	XII
	d	89	(87–92)	$4d^6$-$4d^55f$	89.27	XI
				$4d^6$-$4d^56p$	90.33	XI
	e	95	(92–98)	$4d^7$-$4d^65f$	97.09	X
	f	99	(98–100)	$4d^7$-$4d^66p$	100.61	X
	g	104	(102–107)	$4d^8$-$4d^75f$	106.43	IX

TABLE II. Weighted mean energy, variance, full width at half maximum (FWHM), and skewness of $4d^N$-$4d^{N-1}5f$ and $4d^N$-$4d^{N-1}6p$ transitions in ionized Sn, Sb, Te, and I.

Element		Tin				Antimony				Tellurium				Iodine			
Transition		μ_1 (eV)	σ (eV)	ΔE (eV)	α^3	μ_1 (eV)	σ (eV)	ΔE (eV)	α_3	μ^1 (eV)	σ (eV)	ΔE (eV)	α_3	μ_1 (eV)	σ (eV)	ΔE (eV)	α_3
$4d$-	$5f$	159.382	0.6406	1.885	1.95	176.447	0.850	2.171	1.277	194.139	1.113	2.485		212.457	1.445	2.831	−1.151
	$6p$													232.926	0.465	1.606	12.621
$4d^2$-$4d$	$5f$	149.079	1.832	3.187	−0.101	165.896	2.111	3.422	0.489	183.343	2.453	3.688	−0.130	201.419	2.852	3.976	0.727
	$6p$	154.902	1.855	3.208	−0.396	174.727	2.059	3.379	−0.508	195.529	2.273	3.551	0.729	217.304	2.523	3.741	−0.499
$4d^3$-$4d^2$	$5f$	138.422	4.121	4.780	−0.717	154.980	4.646	5.076	−0.197	172.174	5.182	5.360	−0.551	190.000	5.824	5.683	−1.743
	$6p$	140.949	5.056	5.295	−0.440	160.182	5.561	5.553	−0.820	180.397	6.107	5.820	−1.292	201.588	6.652	6.074	−1.748
$4d^4$-$4d^3$	$5f$	127.892	6.385	5.950	−0.744	144.194	5.621	5.583	−0.206	161.143	6.293	5.907	−0.238	178.722	6.945	6.205	−0.109
	$6p$	127.503	6.248	5.886	−0.176	146.150	6.875	6.174	−0.402	165.784	7.516	6.456	−0.509	186.398	8.098	6.701	0.608
$4d^5$-$4d^4$	$5f$	117.373	5.898	5.719	−0.873	133.419	7.057	6.255	−1.2803	150.060				167.359	7.406	6.406	1.811
	$6p$	114.275	6.715	6.102	−0.273	132.240	7.520	6.457	−0.436	151.383	8.080	6.694	−0.327	171.419	8.777	6.977	−0.500
$4d^6$-$4d^5$	$5f$	106.774	5.742	5.643	−0.690	122.522	6.299	5.910	0.221	138.908	7.416	6.412	−0.619	155.933	7.410	6.410	−0.012
	$6p$	101.349	6.432	5.972	0.318	118.813	7.128	6.287	0.007	137.277	7.838	6.593	−0.353	156.732	8.488	6.861	0.374
$4d^7$-$4d^6$	$5f$	96.001	5.755	5.649	−0.688	111.51				127.717	6.337	5.928	−0.682	144.602	6.949	6.207	−1.296
	$6p$	88.368	6.543	6.023	0.381	104.625				123.249	7.020	6.240	0.188	142.122	7.697	6.533	0.316
$4d^8$-$4d^7$	$5f$	85.450	3.901	4.651	−0.730	100.677	4.29	4.877	−0.380	116.509	4.749	5.132	−0.663	133.030	5.209	5.374	−0.168
	$6p$	76.007	4.031	4.728	0.652	92.273	4.497	4.994	0.701	109.556	4.983	5.257	−0.820	127.845	5.511	5.528	0.415
$4d^9$-$4d^8$	$5f$					89.663	2.694	3.865	−1.074	105.244	3.013	4.087	−1.028	121.421	3.353	4.3121	−0.815
	$6p$	63.645	2.327	3.592	1.140	79.300	2.628	3.817	1.093	95.979	2.939	4.037	1.129	113.508	2.627	3.817	1.093
$4d^{10}$-$4d^9$	$5f$									94.553	1.327	2.713	−4.497	110.689	2.402	3.650	−3.223
	$6p$									82.902	0.258	1.196	−1.1432	99.996	0.323	1.339	0.34

coefficient α_3, which is given by $\alpha_3 = \mu_3^c/(V)^{3/2}$, where μ_3^c is the centered third-order moment and is equal to $\mu_3 - 3\mu_2^c\mu_1 - \mu_1^3$. The normalized intensity of an array is then equal to

$$\left[1 - \frac{\alpha_3\left[x - \dfrac{x^3}{3}\right]}{2} \right] \exp\left[-\frac{x^2}{2} \right] ,$$

where $x = E/\sigma$ is the reduced energy. When dealing with level distributions within configurations, it has been shown to be also convenient to use

$$K_1 = \mu_3^c/V^{3/2} \quad \text{and} \quad K_2 = \mu_4^c/V^2 - 3 .$$

The sign of the skewness, K_1, describes the asymmetry of the configuration being positive when the distribution is biased towards lower energy, negative when the bias is towards higher energy. The excess, K_2, characterizes the level density by comparison with a normal distribution. The value of these quantities in assessing spectral distributions has been dealt with in considerable detail by Kučas and Karazija [29,30,42]. In the present case the wavelengths from the earlier line-by-line calculations were converted into energy in units of eV, the first three moments were calculated for each array, and values of weighted mean, variance, full width at half maximum, and skewness coefficient are given in Table II.

Finally, to complete our description of the UTA, the level and line statistics were explored again using the methodology proposed by Bauche and Bauche-Arnoult [43]. In this scheme the moments of the m_j distribution are evaluated for the upper and lower configurations and from these the distribution of levels within these configurations as well as the approximate number of lines may be evaluated. The first step is to obtain the variance

and fourth-order moment of the m_j distribution. The coefficient of Kurtosis $\mu_4(\mu_2)^{-2}$ will be equal to 3 (excess equal to zero) for a Gaussian distribution. From the values of μ_2 and μ_4 the number of lines can be calculated directly if the exact number of m_j states in the upper and lower configurations is known. But for any configuration the number of states

$$N_s = \prod_{i=1}^{q} \begin{bmatrix} 4l_i + 2 \\ N_i \end{bmatrix} ,$$

where q is the number of open subshells in the configuration N_i. The results of these calculations are presented in Table III. As expected, the larger the number of levels, the closer the distribution approaches Gaussian.

CONCLUSION

We have explored the behavior of weak $4d^N\text{-}4d^{N-1}(5f + 6p)$ arrays in the spectra of ionized tin, antimony, tellurium, and iodine. We have shown that they give rise to UTA which appear as weak continuum modulation overlaid by weak lines superimposed on the recombination background. We have described the UTA emission profiles within the UTA framework and also examined the level distributions in the configurations involved. Our calculations predict a cancellation of the dipole matrix element for $4d$-$5f$ transitions at the thirteenth spectrum in each case.

ACKNOWLEDGMENTS

TABLE III. Level and line statistics for $4d^N\text{-}4d^{N-1}5f$ and $4d^N\text{-}4d^{N-1}6p$ transitions.

Transition	Variance $V(A)$	Variance $V(B)$	$N_s(A)$	$N_s(B)$	Kurtosis coefficient $\alpha_4(A)$	Kurtosis coefficient $\alpha_4(B)$	Number of lines
$d^9\text{-}d^8f^1$	2.25	8.25	10	630	1.95	2.56	80
$d^8\text{-}d^7f^1$	4.00	9.50	45	1680	2.38	2.63	728
$d^7\text{-}d^6f^1$	5.25	10.25	120	2940	2.52	2.66	2859
$d^6\text{-}d^5f^1$	6.00	10.50	210	3528	2.57	2.67	5540
$d^5\text{-}d^4f^1$	6.25	10.25	252	2940	2.58	2.66	5546
$d^4\text{-}d^3f^1$	6.00	9.50	210	1680	2.57	2.63	2869
$d^3\text{-}d^2f^1$	5.25	8.25	120	630	2.52	2.56	735
$d^2\text{-}d^1f^1$	4.00	6.5	45	140	2.38	2.40	83
$d^1\text{-}f^1$	2.25	4.25	10	14	1.95	1.89	3
$d^9\text{-}d^8p^1$	2.25	4.92	10	270	1.95	2.56	59
$d^8\text{-}d^7p^1$	4.00	6.17	45	720	2.38	2.62	468
$d^7\text{-}d^6p^1$	5.25	6.92	120	1260	2.52	2.66	1735
$d^6\text{-}d^5p^1$	6.00	7.17	210	1512	2.57	2.67	3286
$d^5\text{-}d^4p^1$	6.25	6.92	252	1260	2.58	2.66	3289
$d^4\text{-}d^3p^1$	6.00	6.17	210	720	2.57	2.63	1741
$d^3\text{-}d^2p^1$	5.25	4.92	120	270	2.52	2.66	472
$d^2\text{-}d^1p^1$	4.00	3.17	45	60	2.38	2.39	61
$d^1\text{-}p^1$	2.25	9.17	10	60	1.95	2.06	4

[1] G. O'Sullivan and P. K. Carroll, J. Opt. Soc. Am. **71**, 227 (1981).

[2] D. F. Colombant and G. F. Tonon, J. Appl. Phys. **44**, 3524 (1973).

[3] C. E. Moore, *Atomic Energy Levels*, Natl. Bur. Stand (U.S.) Circ. No. 467 (U.S. GPO, Washington, DC, 1958), Vol. III.

[4] A. M. Crooker and Y. N. Joshi, J. Opt. Soc. Am. **54**, 553 (1964).

[5] M. Even-Zohar and B. S. Fraenkel, J. Phys. B **5**, 596 (1972).

[6] V. Kaufman, J. Sugar, and Y. N. Joshi, J. Opt. Soc. Am. B **5**, 619 (1988).

[7] V. Kaufman and J. Sugar, Phys. Scr. **24**, 738 (1981).

[8] V. Kaufman and J. Sugar, J. Opt. Soc. Am. B **1**, 38 (1984).

[9] V. Kaufman, J. Sugar, Th. A. M. van Kleef, and Y. N. Joshi, J. Opt. Soc. Am. B **2**, 426 (1985).

[10] Y. N. Joshi and Th. A. M. van Kleef, Can. J. Phys. **55**, 714 (1977).

[11] R. P. Srivastava, Y. N. Joshi, and Th. A. M. van Kleef, Can. J. Phys. **55**, 1936 (1977).

[12] Th. A. M. van Kleef and Y. N. Joshi, J. Opt. Soc. Am. **6**, 132 (1979).

[13] Y. N. Joshi, Th. A. M. van Kleef, and C. G. Mahajan, J. Opt. Soc. Am. B **4**, 1306 (1987).

[14] Y. N. Joshi and Th. A. M. van Kleef, J. Opt. Soc. Am. **70**, 1344 (1980).

[15] V. Kaufman, J. Sugar, and J. L. Tech, J. Opt. Soc. Am. **73**, 691 (1983).

[16] Y. N. Joshi and A. J. J. Raassen (private communication).

[17] R. L. Kelly and L. J. Palumbo, Naval Research Laboratories (NRL) Report No. 7599, 1972 (unpublished).

[18] G. O'Sullivan in *Giant Resonances in Atoms, Molecules and Solids*, Vol. 151 of *NATO Advanced Study Institute, Series B: Pysics*, edited by J. P. Connerade, J. M. Esteva, and R. Karnatak (Plenum, New York, 1987).

[19] P. Mandelbaum, M. Finkenthal, J. L. Schwob, and M. Klapisch, Phys. Rev. A **35**, 5051 (1987).

[20] M. Klapisch, J. Bauche, and C. Bauche-Arnoult, Phys. Scr. **T3**, 222 (1983).

[21] C. Bauche-Arnoult, J. Bauche, and M. Klapisch, J. Opt. Soc. Am. **68**, 1136 (1978).

[22] C. Bauche-Arnoult, J. Bauche, and M. Klapisch, Phys. Rev. A **20**, 2424 (1979).

[23] C. Bauche-Arnoult, J. Bauche, and M. Klapisch, Phys. Rev. A **25**, 2641 (1982).

[24] M. Klapisch, E. Meroz, P. Mandelbaum, A. Zigler, C. Bauche-Arnoult, and J. Bauche, Phys. Rev. A **25**, 2391 (1982).

[25] C. Bauche-Arnoult, J. Bauche, and M. Klapisch, Phys. Rev. A **30**, 3026 (1984).

[26] C. Bauche-Arnoult, J. Bauche, and M. Klapisch, Phys. Rev. A **31**, 2248 (1985).

[27] J. Bauche, C. Bauche-Arnoult, and M. Klapisch, Adv. At. Mole. Phys. **23**, 131 (1987).

[28] C. Bauche-Arnoult, and J. Bauche, Phys. Scr. **T40**, 58 (1992).

[29] R. Karazija, Acta. Phys. Hungarica **70**, 367 (1991).

[30] S. Kučas and R. Karazija, Phys. Scr. **47**, 754 (1993).

[31] I. P. Grant, B. J. McKenzie, P. H. Norrington, D. F. Mayers, and N. C. Pyper, Comput. Phys. Commun. **21**, 207 (1980).

[32] J. Sugar and V. Kaufman, Phys. Scr. **26**, 419 (1982).

[33] A. J. J. Raassen, Y. N. Joshi, and J. F. Wyart, Phys. Lett. A **154**, 453 (1991).

[34] J. P. Connerade and M. W. D. Mansfield, Phys. Rev. Lett. **48**, 131 (1982).

[35] C. W. Clark, J. Opt. Soc. Am. B **1**, 626 (1984).

[36] J. E. Hansen, J. Brilly, E. T. Kennedy, and G. O'Sullivan, Phys. Rev. Lett. **63**, 1934 (1989).

[37] R. D. Cowan, J. Opt. Soc. Am. **58**, 808 (1968).

[38] J. E. Hansen, J. Phys. B **5**, 1096 (1972).

[39] S. M. Younger, Phys. Rev. A **22**, 2682 (1980).

[40] G. O'Sullivan, J. Phys. B **15**, L765 (1982).

[41] J. Blackburn, P. K. Carroll, J. T. Costello, and G. O'Sullivan, J. Opt. Soc. Am. **73**, 1325 (1983).

[42] R. Karazrja, *Sums of Atomic Quantities and Mean Characteristics of Spectra* (Mokslas, Vilnius, 1991) (in Russian.)

[43] J. Bauche, and C. Bauche-Arnoult, J. Phys. B **20**, 1659 (1987).